Chemical Science

ROYAL SOCIETY OF CHEMISTRY

EDGE ARTICLE

Cite this: DOI: 10.1039/d4sc06058j

All publication charges for this article have been paid for by the Royal Society of Chemistry

Luminescent cyclometalated gold(III) complexes covalently linked to metal–organic frameworks for heterogeneous photocatalysis†

Jian-Rui Chen,‡[abd] Dongling Zhou,‡[b] Yungen Liu,[c] Mian Li,[ad] Yonghong Xiao,[d] Xiao-Chun Huang *[ad] and Chi-Ming Che *[be]

Received 7th September 2024
Accepted 22nd December 2024

DOI: 10.1039/d4sc06058j

rsc.li/chemical-science

Phosphorescent gold(III) complexes possess long-lived emissive excited states, making them ideal for use as molecular sensors and photosensitizers for organic transformations. Literature reports indicate that gold(III) emitters exhibit good catalytic activity in homogeneous photochemical reactions. Heterogeneous metal–organic framework (MOF)-supported gold(III) photocatalysts are considered to show high recyclability in photochemical reactions and potentially provide new selectivities. Here, we report the design and development of visible-light-absorbing MOF-covalently linked gold(III) photocatalysts. A MOF-supported gold(III) complex exhibits a longer phosphorescence lifetime than its homogeneous counterpart, reaching approximately 110 μs under argon and 12 μs under air when suspended in acetonitrile. This is attributed to the localization of the gold(III) complex within the MOF nano-cages. The MOF-derived gold(III) photosensitizer exhibits good catalytic performance in intramolecular and intermolecular [2 + 2] cycloaddition reactions to construct functionalized cyclobutanes and azetidines, both of which are important building blocks for pharmaceuticals. These photochemical [2 + 2] cycloaddition reactions catalyzed by the gold(III)-MOF are governed by an energy transfer mechanism and do not require redox modulators. Under similar reaction conditions, the crossed [2 + 2] photocycloaddition reaction of two activated alkenes proceeds smoothly, and the cyclobutane product is obtained within 3 hours of irradiation under dilute conditions (0.2 mol dm^{-3} of alkene).

Introduction

Triplet emitters with long phosphorescence lifetimes (τ_{ph}) are attractive for their potential use as photocatalysts in photoredox catalysis and photosensitizers in energy transfer catalysis. Given the electrophilic nature of the gold(III) ion, the frontier orbitals of luminescent gold(III) complexes have a minute metal parentage, so they usually exhibit long-lived ligand-centered phosphorescence (^{3}IL) with lifetimes (at room temperature) of up to hundreds of microseconds;[1] this is significantly longer than the sub-microsecond to several microsecond lifetimes of Ir(III) triplet emitters.[2] In addition, luminescent gold(III) complexes exhibit intersystem crossing with close to 100% efficiency, which is brought about by the large spin–orbit coupling constant of gold (around 5100 cm^{-1}). This allows the conversion of all singlet-excited state molecules into their triplet manifolds. These attractive photophysical properties make luminescent gold(III) complexes good photosensitizers for triplet-energy-transfer-mediated photochemical reactions. It is worth noting that the absorption of gold(III) complexes can be easily tuned to the visible light region through ligand modification.[1b,c] Therefore, gold(III) complexes can be developed as photocatalysts for visible-light-induced organic transformation reactions. It has been reported in the literature that gold(III) emitters exhibit high catalytic activity for homogeneous photochemical reactions.[1]

Exploring the catalytic capabilities of metal–organic frameworks (MOFs) has become a rapidly growing field over the past decade.[3] This is due to the inherently superior properties of MOFs, including hyperreactivity, high porosity, huge internal surface area, and customizable pore sizes.[3,4] The pore-confined nanocages of MOFs provide a valuable platform for selective reaction processes and catalytic innovation.[3,5] MOF-supported

[a]Chemistry and Chemical Engineering Guangdong Laboratory, Shantou, Guangdong, P. R. China. E-mail: xchuang@stu.edu.cn

[b]Department of Chemistry, State Key Laboratory of Synthetic Chemistry, The University of Hong Kong, Pokfulam Road, Hong Kong, P. R. China. E-mail: cmche@hku.hk

[c]Department of Chemistry, Southern University of Science and Technology, Shenzhen 518055, Guangdong, P. R. China

[d]Department of Chemistry and Key Laboratory for Preparation and Application of Ordered Structural Materials of Guangdong Province, Shantou University, Guangdong 515063, P. R. China

[e]Laboratory for Synthetic Chemistry and Chemical Biology Limited, Units 1503-1511, 15/F, Building 17W, Hong Kong Science and Technology Parks, New Territories, Hong Kong SAR, P. R. China

† Electronic supplementary information (ESI) available. See DOI: https://doi.org/10.1039/d4sc06058j

‡ J.-R. Chen and D. Zhou contributed equally to this work.

catalysts are of particular interest due to their ease of recovery and recycling and their potential for efficient large-scale production in organic synthesis.[6] Furthermore, heterogeneous photocatalysts have advantages over homogeneous catalytic systems because their catalytic performance is less susceptible to the solubility and concentration of the photo-catalytically active species. Given the advantages offered by MOF-based heterogeneous catalytic systems, we are interested in exploring the potential of integrating photo-functional gold(III) complexes into MOFs to study photo-redox catalysis and photochemical energy transfer reactions.

Several strategies for implanting catalytically active species into MOFs have been reported. One such approach is the "ion exchange" method, in which a charged catalyst is encapsulated in the pores of a MOF through an ion exchange reaction with the existing counterions present in the parent framework. In 2015, Che and co-workers reported the use of this simple method to construct a series of gold(III)-MOF composites that exhibited high photocatalytic activity for the aerobic oxidation of secondary amines to imines and oxidative C–H functionalization.[7] However, gold(III)-MOFs developed using this method may encounter stability issues because the cationic gold(III) complexes inside the MOF nano-cages may exchange with other cations generated during the reaction. This ion exchange process may lead to the release of the gold(III) complex from the MOF, negatively affecting the reusability of the gold(III) catalyst. Alternatively, following the isoreticular principle, MOFs can be functionalized prior to framework construction; additional linkers covalently bound to gold photosensitizers/photocatalysts are employed in MOF synthesis. This "pre-synthetic functionalization" method allows for the functionalization of targeted MOFs while retaining their basic structure, crystallinity, and porosity to a certain extent. For instance, Toste and co-workers introduced bidentate gold(III) complexes into MOFs using a mixed-linker synthetic strategy.[8] They found that the judicious design of gold(III)-containing biphenyl linkers improved the stability of C^C-based gold(III) complexes relative to their homogeneous gold(III) counterparts. The enhanced stability directly translates into their superior catalytic performance in intramolecular cycloaddition reactions compared to homogeneous gold(III) catalysts. Another approach is to modify the structure of a given MOF by introducing catalysts at the reactive sites mounted on the organic linkers.[9] However, this method poses challenges in preparing a variety of MOF-derived metal complexes because the post-synthetic reaction is performed in the solid state, which brings difficulties to the metalation reaction. In some cases, if additional metal catalysts are used in post-synthetic reactions (such as Pd catalysts used in Suzuki coupling), their complete removal may be difficult. This raises concerns regarding the interpretation of experimental results, as it becomes unclear whether the observed catalytic activity is attributed to residual metal catalysts or to the MOF itself.

We here disclose the solvothermal synthesis of two gold(III)-functionalized MOFs, namely **UiO-68[Au1]$_{1.2–4.5\%}$** and **UiO-68[Au2]$_{2.6\%}$**, following a mixed-linker synthetic strategy. Pincer-type gold(III) complexes were incorporated into terphenyl-based linkers through facile reactions between pendent imidazolium groups and gold(III) chloride complexes. The incorporation of gold(III) complexes in the MOF creates a framework with the same microstructure as that of the parent MOF **UiO-68-Me**, thereby retaining its high porosity and crystallinity but with changes in pore size and surface area. It was found that the phosphorescence lifetime of **Au1** attached to the MOF was significantly increased compared to that of the homogeneous counterpart **Au1**. The reusable heterogeneous gold(III) catalyst exhibits excellent performance for intramolecular and intermolecular [2 + 2] cycloaddition reactions, singlet oxygen-sensitized oxidation reactions, and alkyl halide reductive cyclization reactions under visible light irradiation.

Results and discussion

Synthesis of linkers (H_2TPDC-[Au1], H_2TPDC-[Au2]) and gold(III)-functionalized MOFs

Pincer gold(III) complexes containing N-heterocyclic carbene (NHC) linked to terphenyl dicarboxylic acid ligands, including **H_2TPDC-[Au1]** and **H_2TPDC-[Au2]**, were prepared following a four-step procedure with dimethyl 2′-methyl-[1,1′:4′,1″-terphenyl]-4,4″-dicarboxylate (**H_2TPDC**) as the starting material (Scheme S1†). Pincer gold(III) complexes, **Au1** or **Au2**, are covalently attached to the terphenyl building blocks *via* pendent imidazolium groups. This is easily achieved by refluxing a methanol solution of [Au(C^N^C)Cl], potassium *tert*-butoxide, and terphenyl ligand. The crystal structure of **Me-TPDC-[Au1]** is shown in Scheme 1. Due to steric hindrance, the [Au(C^N^C)] plane adopts a twisted orientation relative to the carbene ligand. The [Au(C^N^C)] fragment is aligned parallel to one of the phenyl rings of the terphenyl unit, with an interplanar contact of about 4.1 Å.

UiO-68-Me is a face-centered cubic topology MOF, which is constructed from $Zr_6O_4(OH)_4$ clusters and terphenyl building units. It was selected for the development of gold(III)-functionalized MOFs for photocatalytic investigations because of its ultrahigh surface area, exceptional thermal stability, high resistance to water and organic solvents, and high stability (the ability to maintain its crystalline structure) even under high-pressure conditions.[10a,b] Furthermore, **UiO-68-Me** has a three-dimensional porous structure with highly ordered distribution of tetrahedral and octahedral cages with calculated pore sizes of

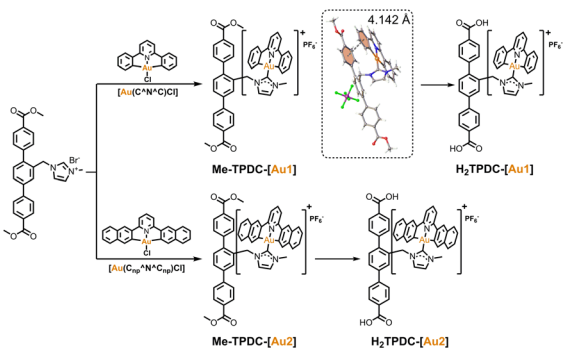

Scheme 1 Synthetic pathways for linkers H_2TPDC-[Au1] and H_2TPDC-[Au2]. (Inset) The crystal structure of Me-TPDC-[Au1].

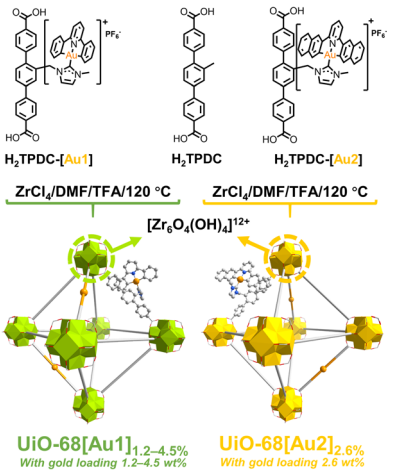

Scheme 2 Synthesis of gold(III)-MOFs **UiO-68[Au1]**$_{1.2–4.5\%}$ and **UiO-68[Au2]**$_{2.6\%}$ using a mixed-linker strategy.

approximately 12 and 14 Å, respectively.[10c] The large cages in **UiO-68-Me** not only provide ample space to accommodate gold(III) complexes but also facilitate the easy diffusion of substrates. Using a mixed-linker synthetic strategy, **UiO-68[Au1]**$_{1.2–4.5\%}$ and **UiO-68[Au2]**$_{2.6\%}$ were successfully synthesized (Scheme 2, see the ESI† for more details). For comparison, **UiO-68-Me** was also prepared according to the reported method.[10d] The current design involves integrating the organogold(III) complex into the terphenyl ligand *via* a pendent imidazolium unit, largely retaining the key terphenyl building blocks in the established **UiO-68** MOFs, which enables the synthesis of gold(III)-functionalized MOFs in a more accessible manner and preserves the high porosity and crystallinity of the parent framework.

Characterization, stability, and porosity

Fig. 1a depicts the powder X-ray diffraction (PXRD) data of the as-synthesized **UiO-68[Au1]**$_{1.2–4.5\%}$ and **UiO-68[Au2]**$_{2.6\%}$, whose diffraction patterns are consistent with the simulated data for **UiO-68-Me**. The comparison suggests that **UiO-68[Au1]**$_{1.2–4.5\%}$ and **UiO-68[Au2]**$_{2.6\%}$, developed using the mixed-linker synthetic protocol, largely maintain the highly ordered structure of the parent framework **UiO-68-Me**. The morphologies and particle sizes of **UiO-68[Au1]**$_{1.2–4.5\%}$ and **UiO-68[Au2]**$_{2.6\%}$ were characterized using field-emission scanning electron microscopy (FE-SEM).

Fig. S1† shows the octagon-like structures of these gold(III)-MOFs. Notably, the average particle sizes of **UiO-68[Au1]** decrease from 20 to 9 μm upon changing the feed ratio of linkers **H$_2$TPDC-[Au1]** and **H$_2$TPDC** used in the MOF synthesis from 1 : 20 to 1 : 5. It can be speculated that the growth of **UiO-68[Au1]** crystal sizes may be impeded by the high concentration of the linker **H$_2$TPDC-[Au1]** during the crystallization process.

The chemical composition and metal distribution of these MOFs were characterized using energy-dispersive X-ray

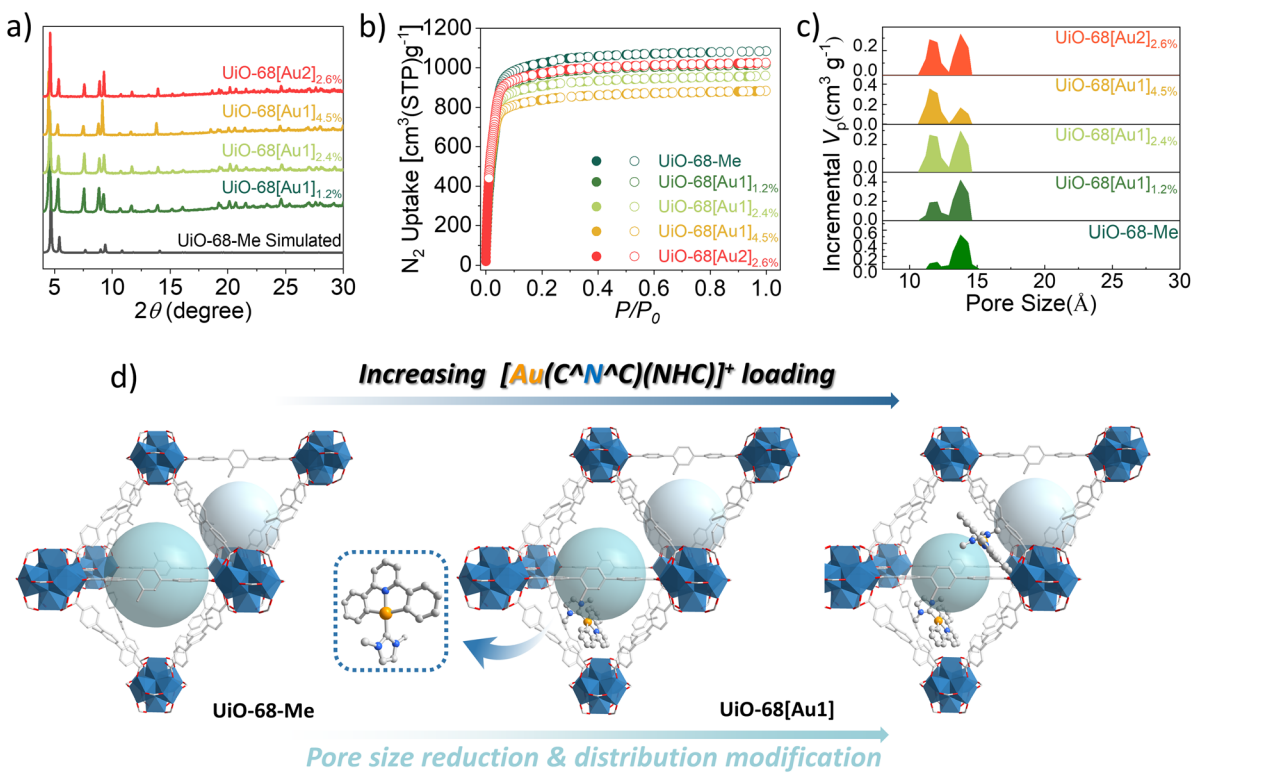

Fig. 1 (a) Experimentally obtained PXRD patterns of **UiO-68[Au1]**$_{1.2–4.5\%}$ and **UiO-68[Au2]**$_{2.6\%}$ and the simulated pattern of **UiO-68-Me**; (b) N_2 sorption isotherms of **UiO-68-Me**, **UiO-68[Au1]**$_{1.2–4.5\%}$ and **UiO-68[Au2]**$_{2.6\%}$ at 77 K; (c) pore size distribution of **UiO-68-Me**, **UiO-68[Au1]**$_{1.2–4.5\%}$ and **UiO-68[Au2]**$_{2.6\%}$ analyzed using the NLDFT method based on nitrogen adsorption measurements; (d) illustration of the effect of increasing the loadings of gold(III) complexes on pore size distributions.

spectroscopy (EDS), X-ray photoelectron spectroscopy (XPS), and inductively coupled plasma-atomic emission spectroscopy (ICP-MS). The measurement of SEM coupled with EDS elemental mapping shows **UiO-68[Au1]$_{1.2–4.5\%}$** and **UiO-68[Au2]$_{2.6\%}$** with an even distribution of Au, Zr, C, and O (Fig. S2–5†). Even when using low feed ratios of gold(III)-modified linkers **H_2TPDC-[Au1]** and **H_2TPDC-[Au2]**, the observed uniform distribution of Au in **UiO-68[Au1]$_{1.2\%}$** and **UiO-68[Au2]$_{2.6\%}$** suggests the feasibility of the mixed-linker synthetic method employed for gold(III)-functionalized **UiO-68** MOFs. XPS analysis was conducted to determine the oxidation state of Au species in **UiO-68[Au1]$_{4.5\%}$** and **UiO-68[Au2]$_{2.6\%}$** as representatives. As shown in Fig. S6,† their Au $4f_{7/2}$ photoelectron peaks are located at binding energy values of 84.2–84.6 eV, which are comparable to the Au $4f_{7/2}$ peaks of the respective gold(III) chloride complexes (85.2 eV), revealing that gold(III) complexes are present in **UiO-68[Au1]$_{4.5\%}$** and **UiO-68[Au2]$_{2.6\%}$**. ICP-MS analysis shows the Au : Zr ratios of 1 : 25.6, 1 : 13.1, 1 : 6.3, and 1 : 15.1 for **UiO-68[Au1]$_{1.2\%}$**, **UiO-68[Au1]$_{2.4\%}$**, **UiO-68[Au1]$_{4.5\%}$**, and **UiO-68[Au2]$_{2.6\%}$**, respectively (Table S2†). These characterization efforts collectively demonstrate the successful construction of gold(III)-MOFs using the mixed-linker synthetic protocol.

The digestion experiment, accompanied by NMR analysis, offers an effective way to verify the constituent building blocks in mixed-linker MOFs. In this study, **UiO-68[Au1]$_{1.2–4.5\%}$** and **UiO-68[Au2]$_{2.6\%}$** were subjected to digestion under K_3PO_4/D_2O/DMSO-d_6, and subsequently, clear solutions were obtained. The ^{1}H NMR spectra of digested **UiO-68[Au1]$_{1.2–4.5\%}$** and **UiO-68[Au2]$_{2.6\%}$** solutions indicate the presence of intact gold(III)-substituted terphenyl ligands (Fig. S10 and 11†), revealing that the gold(III)-functionalized linkers are released from the MOFs due to the decomposition of Zr-based clusters by tripotassium phosphate. The digestion experiment showed a lower percentage of gold(III)-functionalized linkers in the MOF compared to the percentage used in the feed ratio for MOF synthesis. **UiO-68[Au1]$_{4.5\%}$** exhibited good stability, maintaining its high crystallinity and structural integrity when exposed to various organic solvents as well as acidic (pH 3–5) and basic (pH 9–11) solutions. Its robustness was even evident under high-temperature conditions (100 °C for 6 h). These results are illustrated in Fig. S12 and S16.† **UiO-68[Au1]$_{4.5\%}$** was treated with $NaBH_4$, and the resulting MOF sample was subjected to TEM and XPS analysis. TEM characterization shows particle aggregation within the MOFs, and XPS analysis suggests the presence of Au(0) in the MOFs (Fig. S8 and S9†).

In order to study the porosity of gold(III)-MOFs, the single-component equilibrium adsorption behaviors of activated MOFs were studied in detail. The MOF was activated through solvent exchange using MeCN and then thermally treated at 100 °C under vacuum. PXRD studies show that the crystallinity of MOFs can be maintained after thermal treatment (Fig. S13–S17†). The permanent porosity of **UiO-68-Me** and gold(III)-functionalized MOFs was evaluated through nitrogen gas sorption measurements at 77 K and 1 bar (Fig. 1b and Table S3†). **UiO-68-Me**, **UiO-68[Au1]$_{1.2–4.5\%}$**, and **UiO-68[Au2]$_{2.6\%}$** show typical reversible type I adsorption–desorption isotherms of nitrogen at 77 K (Fig. 1b), indicating their microporous structure. Activated **UiO-68-Me** shows a N_2 volumetric uptake of 1081 cm^3 g^{-1} (at $P/P_0 = 0.9$), corresponding to a pore volume of 1.67 cm^3 g^{-1} and a Brunauer–Emmett–Teller (BET) surface area of 4323 cm^2 g^{-1}. These values are comparable to those reported in the literature.[10d] Compared with the parent framework **UiO-68-Me**, lower N_2 sorption was observed for **UiO-68[Au1]$_{1.2–4.5\%}$** and **UiO-68[Au2]$_{2.6\%}$**, showing reduced pore volume (1.36–1.58 cm^3 g^{-1}) and BET surface area (3471–3947 cm^2 g^{-1}). Interestingly, increasing the gold content in **UiO-68[Au1]** from 1.2 to 4.5 wt%

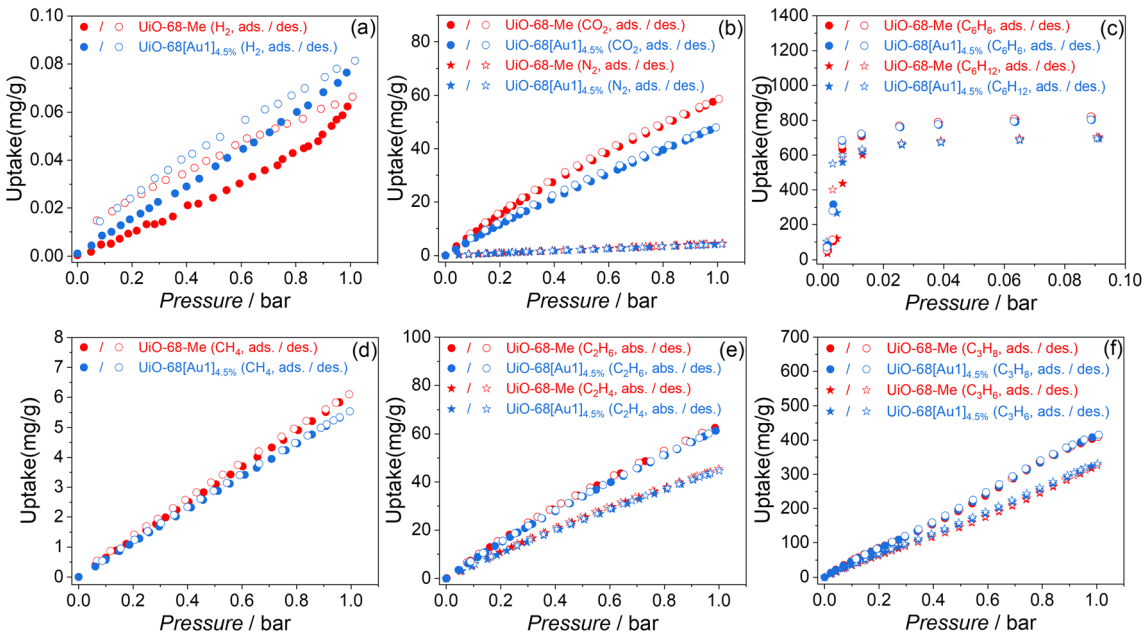

Fig. 2 Single-component sorption isotherms for (a) H_2, (b) CO_2 and N_2, (c) C_6H_6 and C_6H_{12}, (d) CH_4, (e) C_2H_4 and C_2H_6, and (f) C_3H_6 and C_3H_8 of **UiO-68-Me** and **UiO-68[Au1]$_{4.5\%}$** at 298.15 K. "Ads" and "des" stand for adsorption and desorption, respectively.

results in a further decrease in the BET surface area and pore volume of the MOFs. Based on these experimental findings, it can be inferred that pendent gold(III) complexes tend to be located in the micropores of MOFs. The pore size distributions of **UiO-68-Me**, **UiO-68[Au1]$_{1.2–4.5\%}$**, and **UiO-68[Au2]$_{2.6\%}$** were derived from experimental sorption data by fitting the isotherms using the NLDFT model. **UiO-68-Me** has two different sizes of cages: a tetrahedral cage (12 Å) and an octahedral cage (14 Å). When the pincer gold(III) complex **Au1** was grafted onto the MOF linker, the distribution of pores with a size of 14 Å gradually decreased as the content of **Au1** increased (Fig. 1c). The trend is evident in the results for **UiO-68[Au1]$_{1.2–4.5\%}$**. These data reveal the preferential location of **Au1** within the octahedral cage, thereby reducing the respective pore size, as shown in Fig. 1d.

The porous structure of MOFs features a high surface area, allowing them to efficiently adsorb small molecules. The kinetic adsorption capacity of **UiO-68-Me** and **UiO-68[Au1]$_{4.5\%}$** towards other small molecules was further examined for comparison under pressures up to 0.1 or 1.1 bar at 298.15 K (Fig. 2). The results show that **UiO-68[Au1]$_{4.5\%}$**, which has narrower pore sizes compared to **UiO-68-Me**, is ineffective for selective molecule sieving of C_2H_6/C_2H_4, C_3H_8/C_3H_6, and C_6H_6/C_6H_{12}. However, when comparing the adsorption capacities of **UiO-68-Me** and **UiO-68[Au1]$_{4.5\%}$** for CH_4, C_2H_6, and C_3H_8 (Fig. 2d–f), there is an interesting observation: compared with **UiO-68-Me**, **UiO-68[Au1]$_{4.5\%}$** exhibits a lower CH_4 uptake, while showing a comparable uptake capacity for C_2H_6 and a higher adsorption capacity for C_3H_8. These behaviors exhibited by **UiO-68[Au1]$_{4.5\%}$** may be attributed to the increased C–H/π interactions between gas molecules within the **UiO-68[Au1]$_{4.5\%}$** pores and the aromatic rings of $[Au(C^N^C)(NHC)]^+$; the order is $C_3H_8 > C_2H_6 > CH_4$.[11] Hydrogen is a green energy carrier, and the H_2 storage capability of MOFs has been actively studied.[12] In this work, the H_2 uptake of **UiO-68[Au1]$_{4.5\%}$** was slightly higher (0.081 mg g^{-1} at 1 bar) compared to that of **UiO-68-Me** (0.066 mg g^{-1} at 1 bar), as shown in Fig. 2a.

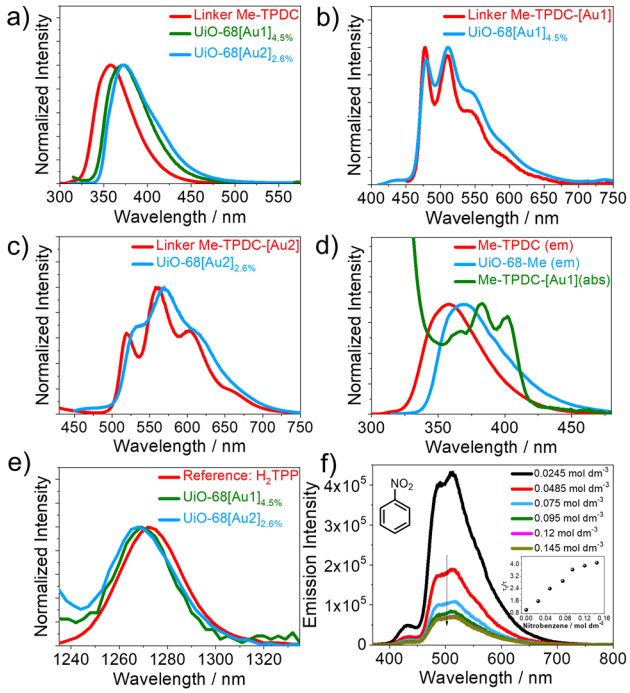

Fig. 3 (a) Fluorescence spectra of gold(III)-MOFs and the unsubstituted terphenyl building unit recorded with an excitation wavelength at 290 nm; (b and c) emission spectra of **Me-TPDC-[Au1]** and **Me-TPDC-[Au2]** dissolved in degassed MeCN and emission spectra of **UiO-68[Au1]$_{4.5\%}$** and **UiO-68[Au2]$_{2.6\%}$** suspended in MeCN under argon, with an excitation wavelength of 380 nm for (b) and 390 nm for (c); (d) absorption spectrum of **Me-TPDC-[Au1]** in MeCN and emission spectra of **Me-TPDC** in MeCN and **UiO-68-Me** suspended in MeCN; (e) singlet oxygen emission spectra generated by 5,10,15,20-tetraphenylporphyrin (H_2TPP) used as a reference and by **UiO-68[Au1]$_{4.5\%}$** and **UiO-68[Au2]$_{2.6\%}$** in oxygen-saturated MeCN; (f) emission spectra of **UiO-68[Au1]$_{2.4\%}$** (suspended in MeCN) in the presence of different concentrations of nitrobenzene (0.0245–0.145 mol dm^{-3}), with an excitation wavelength of 355 nm; inset: plot of emission quenching of **UiO-68[Au1]$_{2.4\%}$** by nitrobenzene at different concentrations.

Photophysical properties

As shown in Fig. S19,† the UV-visible diffuse reflectance spectrum of **UiO-68[Au1]$_{4.5\%}$** shows additional absorption bands in the lower-energy region of 380–430 nm. This is somewhat different from **UiO-68-Me**, whose absorption band extends to around 400 nm. Notably, the low-energy structured absorption bands observed in **UiO-68[Au1]$_{4.5\%}$** are similar in profile and energy to those found in the corresponding homogeneous gold(III) complex counterpart **Au1**. This finding also provides evidence for the successful introduction of gold(III) complexes into MOF matrices.

Upon photoexcitation, **UiO-68[Au1]$_{1.2–4.5\%}$** and **UiO-68[Au2]$_{2.6\%}$** exhibit dual emissions at room temperature when suspended in deoxygenated MeCN, with the higher-energy emission band peaking at around 370 nm and the other located in the green (or yellow) energy region (Fig. 3a–c). Table 1 summarizes the phosphorescence lifetime (τ_{ph}), emission quantum yield (Φ_{ph}, Φ_F), and emission energy ($\tau_{em,\ ph}$) of the gold(III)-MOFs investigated in this work. Since the emission maximum, spectral profile, and nanosecond emission lifetime (<10 ns) of the blue emission band are very similar to those of the terphenyl linker **Me-TPDC**, the emission band centered at around 370 nm can be reasonably attributed to fluorescence derived from the terphenyl skeleton of gold(III)-MOFs. The lower-energy vibronic emission bands (E_{0-0} of 477–532 nm) of these gold(III)-MOFs resemble the emission energy of their respective homogeneous gold(III) carbene complexes (*i.e.* **Au1** and **Au2**).[13] Together with small radiative decay rate constants on the order of 10^2 s^{-1} and long emission lifetimes of up to 110 μs, which are typical traits of ^{3}IL-emitting gold(III) complexes,[1] the lower-energy structured emission bands correspond to phosphorescence originating from the ^{3}IL excited state of the MOF pendent gold(III) complex.

It was found that the functionalization of **UiO-68-Me** with gold(III) complexes (**Au1** or **Au2**) profoundly suppressed the fluorescence originating from the terphenyl skeleton, and Φ_F decreased from 95.6% in **UiO-68-Me** to less than 20% in **UiO-68**

Table 1 Photophysical properties of linkers (**Me-TPDC-[Au1]** and **Me-TPDC-[Au2]**) and MOFs (**UiO-68-Me**, **UiO-68[Au1]$_{1.2–4.5\%}$** and **UiO-68[Au2]$_{2.6\%}$**) studied in this work[a]

MOFs/compound	Conditions	$\lambda_{em,\ ph}$ (nm)	Φ_{ph} (%)	τ_{ph} (μs)	$\lambda_{em,\ F}$ (nm)	Φ_F[b] (%)
UiO-68[Au1]$_{4.5\%}$	Air	479, 511, 545(sh)	0.3	12.1	372	4.1
	Degassed		1.3	56.9		
UiO-68[Au1]$_{2.4\%}$	Air	479, 511, 545(sh)	<0.1	1.14	375	12.3
	Degassed		1.2	41.5		
UiO-68[Au1]$_{1.2\%}$	Air	477, 511, 549(sh)	<0.1	1.35	374	16.2
	Degassed		2.2	113.3		
UiO-68[Au2]$_{2.6\%}$	Air	532, 569, 613(sh)	<0.1	0.02	373	15.3
	Degassed		2.2	103.0		
UiO-68-Me	Air				369	95.6
Me-TPDC-[Au1]	Air	478, 510, 543(sh)	<0.1	0.4		
	Degassed		0.3	1.3		
Me-TPDC-[Au2]	Air	520, 560, 602	<0.1	0.9		
	Degassed		3.6	178.5		
Me-TPDC	Air				358	58.5

[a] For the measurements, the MOFs were suspended in MeCN, and the gold(III) complexes were dissolved in MeCN at a concentration of 2×10^{-5} mol dm^{-3}; $\lambda_{em,\ ph}$ and $\lambda_{em,\ F}$ refer to phosphorescence and fluorescence emission maxima, respectively; Φ_{ph} and Φ_F denote phosphorescence and fluorescence quantum yields, respectively; τ_{ph} represents phosphorescence lifetime; "sh" stands for shoulder; values of Φ below 0.001 fall outside instrumental accuracy. [b] Fluorescence quantum yields (Φ_F) were recorded with the samples exposed to air.

[Au1]$_{1.2–4.5\%}$ and **UiO-68[Au2]$_{2.6\%}$**. As shown in Fig. 3d, the emission spectrum of the terphenyl linker **Me-TPDC** has significant spectral overlap with the absorption spectrum of **Me-TPDC-[Au1]**, showing that the energy transfer process from the terphenyl fragment to **Au1** is feasible. This may be the reason for the reduced fluorescence intensity observed in **UiO-68 [Au1]$_{1.2–4.5\%}$** and **UiO-68[Au2]$_{2.6\%}$** compared to **UiO-68-Me**. Upon increasing the **Au1** content in **UiO-68[Au1]** from 1.2 wt% to 4.5 wt%, the blue fluorescence intensity further decreases, with Φ_F reducing from 16% to 4%. This may be due to the reduced molecular distance between the terphenyl unit (as an energy donor) and **Au1** (as an energy acceptor), leading to more efficient energy transfer. Compared with the terphenyl ligand **Me-TPDC**, two gold(III)-substituted linkers, **Me-TPDC-[Au1]** and **Me-TPDC-[Au2]**, also show reduced fluorescence intensity.

Incorporating the gold(III) complex **Au1** into MOFs has been shown to significantly increase the τ_{ph} of **Au1**, as shown in Table 1. Under degassed conditions, the τ_{ph} of **UiO-68[Au1]$_{1.2–4.5\%}$** (42–110 μs) is more than 30 times longer than the τ_{ph} of **Au1** in MeCN (1.3 μs). It has been reported that the emission lifetime increases when gold(III) complexes are encapsulated in MOFs using a cation exchange method.[7] Notably, the phosphorescence emission of **UiO-68[Au1]$_{4.5\%}$** exhibits less susceptibility to oxygen quenching compared to **UiO-68[Au1]$_{1.2–2.4\%}$**. When exposed to air, the τ_{ph} of **UiO-68[Au1]$_{4.5\%}$** decreased by five times, whereas the τ_{ph} of **UiO-68[Au1]$_{1.2\%}$** and **UiO-68[Au1]$_{2.4\%}$** decreased by approximately 80 and 40 times, respectively. The different responses to oxygen quenching observed in **UiO-68 [Au1]$_{1.2–4.5\%}$** may be due to differences in their nano-space dimensions. As mentioned above, **UiO-68[Au1]$_{4.5\%}$** has the smallest pore volume and BET surface area among **UiO-68[Au1]**. The reduction of nano-cages may help prevent oxygen diffusion into the MOF cage, thereby effectively suppressing the phosphorescence quenching of **UiO-68[Au1]$_{4.5\%}$** by oxygen.

Considering that **UiO-68[Au1]$_{1.2–4.5\%}$** and **UiO-68[Au2]$_{2.6\%}$** have long triplet excited state lifetimes and relatively high triplet energy with E_{0-0} at 477–532 nm (2.33–2.60 eV) compared to the $^1O_2$ phosphorescence emission energy (λ_{em} at around 1 eV), these MOF-supported gold(III) complexes are of appeal for serving as $^1O_2$-generating photosensitizers upon visible light irradiation. In this regard, the generation of $^1O_2$ under light irradiation of **UiO-68[Au1]$_{4.5\%}$** and **UiO-68[Au2]$_{2.6\%}$** was examined. Fig. 3e shows the $^1O_2$ emission spectrum centered at around 1270 nm, which was recorded with an oxygen-saturated MeCN suspension of gold(III)-MOFs under 380 nm light irradiation. The recorded $^1O_2$ emission demonstrates that these gold(III)-MOFs can serve as heterogeneous photosensitizers for singlet oxygen evolution in photocatalytic reactions. The subsequent sections will delve into the photochemical oxidation reaction mediated by gold(III)-MOFs.

As **UiO-68[Au1]** has a relatively long triplet lifetime compared to its homogeneous counterpart **Au1**, we studied the emission quenching of **UiO-68[Au1]$_{2.4\%}$** suspended in MeCN in the presence of nitrobenzene under air. The addition of nitrobenzene resulted in emission quenching of **UiO-68[Au1]$_{2.4\%}$** without any change in the emission maximum (Fig. 3f). Significant emission quenching occurs at nitrobenzene concentrations in the range of 0.0245–0.075 mol dm^{-3}, and then, as the analyte concentration further increases, the quenching shows a trend toward a maximum. This observation may be a result of diffusion control within the MOF pores.

Photo-catalytic organic transformation reactions

To evaluate the photoreactivity and recyclability of the as-prepared gold(III)-MOFs, their utility as photocatalysts in various reactions, including [2 + 2] cycloaddition, singlet oxygen-sensitized oxidation reaction, and alkyl bromide reductive cyclization, was investigated. Our research begins with the

light-driven alkene [2 + 2] cycloaddition reaction. This reaction is the premier method for constructing cyclobutanes, which are prevalent among successful drug candidates.[14] The formation of cyclobutane from alkenes can be achieved through photosensitized energy transfer[15] or electron transfer[16] mechanisms. Our developed **UiO-68[Au1]$_{1.2–4.5\%}$** shows a triplet energy of 62 kcal mol^{-1}, which is determined from the onset of the emission spectrum, as indicated in Fig. 3b. This value indicates that photoexcited **UiO-68[Au1]$_{1.2–4.5\%}$** is capable of energy transfer to those alkenes with relatively low triplet energies of around 50–60 kcal mol^{-1}.[17] According to the excited state reduction potential of **Au1** (referred to as [Au(C^N^C)(NHC)]$^{+}$), where E(Au*/Au^{-}) = +1.29 V (*versus* SCE),[13a] another possible mechanistic scenario involving electron transfer can be ruled out. From a thermodynamic perspective, the alkene substrate examined here, **1e**, which has a first oxidation peak potential of +1.42 V (*versus* SCE),[15a] is hardly oxidized by the excited state of **Au1**. For these reasons, the gold(III)-MOF-mediated light-driven [2 + 2] cycloaddition reaction studied here preferentially proceeds through an energy transfer mechanism rather than an electron transfer pathway.

Initial experiments were performed with **1a** in the presence of catalytic amounts (1 mol%) of **UiO-68[Au1]$_{4.5\%}$** in MeCN for 1 h under 410 nm irradiation. Considering that the long-lived triplet excited state of the gold(III) photosensitizer would be quenched by oxygen, the reaction was carried out under argon to obtain bicyclic compound **2a** in a high yield of 95% and a diastereomeric ratio (d.r.) of 6 : 1, as shown in Table 2. Notably, the yield of **2a** decreased only slightly (by 7%, Table S4†) when the reaction was conducted under air. This marginal decrease can be attributed to the extended emission lifetime of **UiO-68[Au1]$_{4.5\%}$** in the presence of oxygen, approximately 12 μs. Omission of either the photosensitizer **UiO-68[Au1]$_{4.5\%}$** or light irradiation produced only trace amounts of product **2a** (Table S4†), confirming the necessity of both components for the reaction to occur. Using **UiO-68-Me** instead of **UiO-68[Au1]$_{4.5\%}$** resulted in only trace amounts of **2a**. We also compared the catalytic efficiency of **UiO-68[Au1]$_{4.5\%}$** with other widely studied photocatalysts, such as Ir[(dFppy)$_2$dtbbpy]PF$_6$ and thioxanthone. The yields of product **2a** were comparable (Table S4†). As a control, **Au1**-mediated photocycloaddition of **1a** produced **2a** in a comparable yield (96%) under otherwise identical conditions, indicating that the incorporation of **Au1** into the MOF did not alter its catalytic activity (Table S4†). Notably, the incorporation of gold(III) complexes into **UiO-68** MOFs was found to confer a higher degree of stability to the gold(III) catalyst. The supportive findings include: (i) in a 150 min reaction with **1a** (Fig. 5a), the use of **UiO-68[Au1]$_{4.5\%}$** as the catalyst led to the formation of **2a** with a turnover number of 484. This turnover number is at least as good as (if not better than) the 274 turnover number obtained using **Au1**. Notably, the photo-activity of homogeneous **Au1** decreased significantly after 30 minutes of reaction; and (ii) after photolysis, the color of the reaction solution mixture involving **UiO-68[Au1]$_{4.5\%}$** remained unchanged, while the reaction carried out with the homogeneous counterpart **Au1** turned deep purple, indicating that the homogeneous gold(III) catalyst decomposed during the photolysis (Fig. 5c and d).

Table 2 Photo-induced intramolecular [2 + 2] cycloadditions of alkenes enabled by **UiO-68[Au1]$_{4.5\%}$**[a]

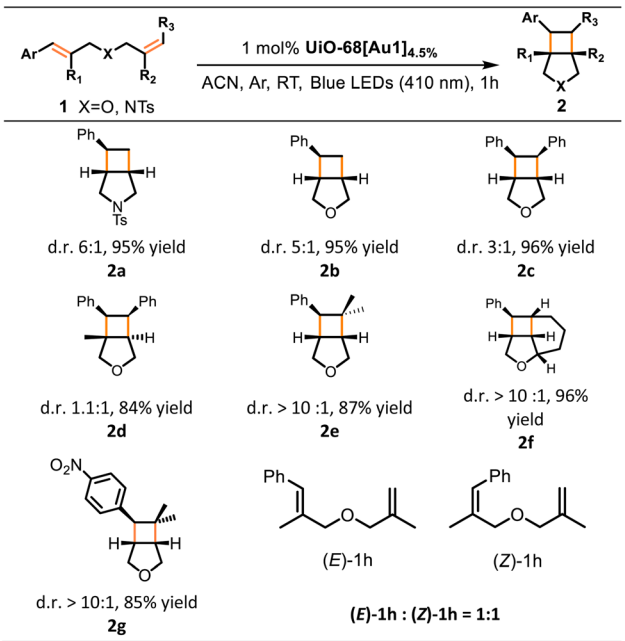

[a] Conditions: reactions were performed with 0.1 mmol of **1a–1h** and 1 mol% **UiO-68[Au1]$_{4.5\%}$** in MeCN (2 mL) at room temperature under argon and 410 nm irradiation for 1 h; product yields and diastereomeric ratios (d.r.) were determined by ^{1}H NMR analysis from the crude product using chlorodiphenylmethane as an internal standard.

In order to verify the reaction mechanism, an emission quenching experiment was performed on **Au1** with increasing concentration of **1a** (Fig. 4a). A linear correlation with the concentration of **1a** was observed with a quenching rate constant (k_q) of 4.1 × 10^9 dm^3 mol^{-1} s^{-1}, suggesting that the quenching of the triplet excited state of **Au1** by **1a** could occur upon light irradiation. The nanosecond transient absorption difference (ns-TA) spectrum of **Au1** in the presence of **1a** was recorded and is shown in Fig. 4b. This spectrum shares a common profile with the TA spectrum of **Au1** only (Fig. 4c). The main distinguishing feature between these two TA spectra (Fig. 4b and c) is the decay lifetime of the absorption band. Specifically, after adding **1a**, the decay lifetime of the absorption band at 440 nm is reduced from 0.76 μs to 0.4 μs, which is consistent with the large k_q obtained in the quenching experiment. The reaction mechanism is shown in Fig. S21.† Upon visible light irradiation, the gold(III) catalyst is excited to the singlet excited state and then undergoes rapid intersystem crossing to reach its triplet manifold. The reactive triplet state of alkene **1a** is accessed through a Dexter-type energy transfer process from the triplet excited state of the gold(III) catalyst to the alkene substrate. The resulting triplet-excited-state alkene reacts with the ground-state alkene to form a biradical intermediate, which undergoes ring closure to yield bicyclic cycloaddition product **2a**.

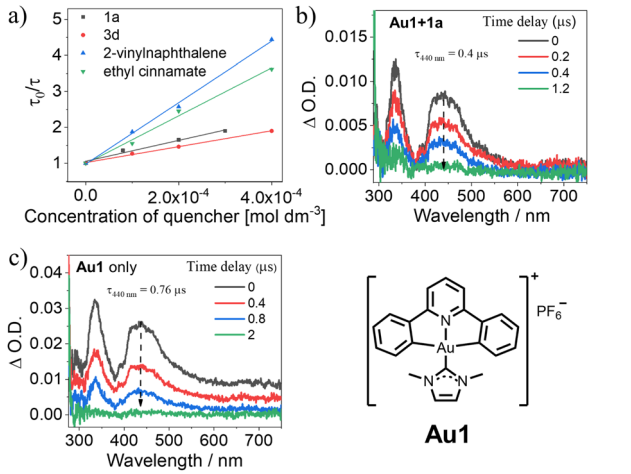

Fig. 4 (a) Stern–Volmer plots of emission quenching of **Au1** (2×10^{-5} mol dm^{-3} in MeCN) by different substrates. The fitted k_q values for **Au1** upon addition of **1a**, **3d**, 2-vinylnaphthalene (**6b**), or ethyl cinnamate (**6a**) are 4.1×10^9, 3.0×10^9, 1.1×10^{10}, or 8.7×10^9 dm^3 mol^{-1} s^{-1}, respectively; (b) ns-TA spectrum of **Au1** (2×10^{-5} mol dm^{-3}) in the presence of **1a** (3×10^{-4} mol dm^{-3}); (c) ns-TA spectrum of **Au1** only (2×10^{-5} mol dm^{-3}).

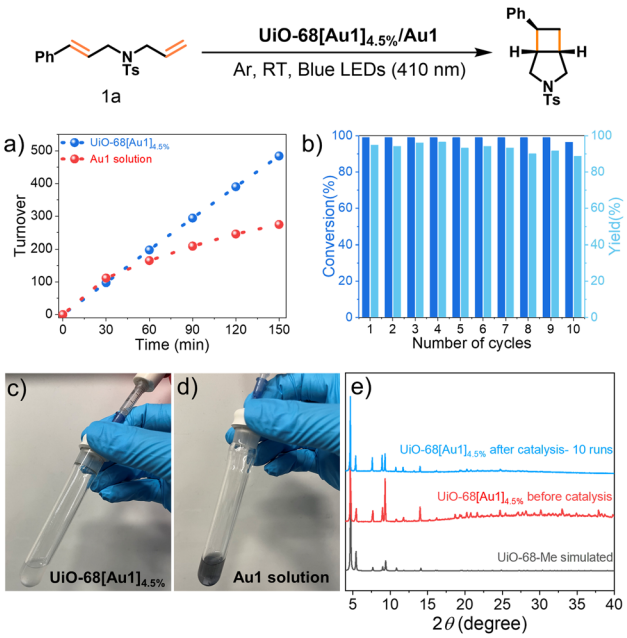

Fig. 5 (a) Product turnovers in the [2 + 2] cycloaddition of **1a** to **2a** by UiO-68[Au1]$_{4.5\%}$ or **Au1** (referring to [Au(C^N^C)(NHC)]PF6); (b) substrate conversion and product yield in recycling experiments with ten reaction cycles using UiO-68[Au1]$_{4.5\%}$ as the photocatalyst in the given reaction; (c and d) photographs of the photocycloaddition of **1a** involving UiO-68[Au1]$_{4.5\%}$ or **Au1**, taken after the reaction; (e) PXRD patterns of UiO-68-Me (simulated) and UiO-68[Au1]$_{4.5\%}$ before and after catalysis (measured).

The cycling stability of the heterogeneous photocatalyst **UiO-68[Au1]$_{4.5\%}$** was evaluated. **UiO-68[Au1]$_{4.5\%}$** can be readily recycled through washing with MeCN for subsequent reactions. After ten consecutive reaction cycles, both the substrate (**1a**) conversion and product yield retained high values of 96% and 89%, respectively (Fig. 5b). The remarkable recyclability and catalytic activity of gold(III)-MOF may be attributed to its high stability under the reaction conditions used. A comprehensive stability assessment of the recycled **UiO-68[Au1]$_{4.5\%}$** was performed using PXRD, XPS, ICP-MS, SEM, and TEM measurements. PXRD analysis demonstrated that the recycled **UiO-68[Au1]$_{4.5\%}$** maintained high crystallinity and structural integrity (Fig. 5e). Comparison of the XPS spectra of **UiO-68[Au1]$_{4.5\%}$** before and after ten catalytic runs showed no significant differences in the peak profiles and Au 4f binding energy values associated with the gold(III) oxidation state (Fig. S23†). ICP-MS analysis indicated minimal leaching (only 4%) of **Au1** from the MOFs (Table S5†). SEM and TEM images of **UiO-68[Au1]$_{4.5\%}$** showed that gold nanoparticles were not deposited onto the MOF surface. The gold(III) complex appears to remain well-contained within the MOF structure. As shown in Fig. S24 and S25,† a decrease in the particle size of the MOF was observed after ten reaction runs, and the decrease in particle size did not seem to compromise the catalytic performance of the MOF to some extent. To highlight the effect of the **Au1** catalyst covalently linked to the MOF, **UiO-68-Me** and **Au1** were physically combined and the resulting mixtures were subjected to catalytic studies for comparison. When this physically mixed system was used to replace **UiO-68[Au1]$_{4.5\%}$** as the photosensitizer, the substrate conversion and product yields of **2a** dropped significantly to around 30% after two reaction runs (Fig. S26†).

The substrate scope of the **UiO-68[Au1]**-catalyzed intramolecular cycloadditions of alkenes was examined. As shown in Table 2, styrene derivatives (**1b–1g**) containing different functional groups underwent [2 + 2] cycloaddition smoothly, and the bicyclic products **2b–2g** were obtained in high yields (84–96%). It is worth noting that the sterically demanding substituents do not impede the reaction (products **2d** and **2e**). Notably, when using the substrate **(*E*)-1h** in which R_1 and R_2 are both methyl groups, ^{1}H NMR analysis after irradiation showed no evidence of the desired cyclobutane product, instead a mixture of **(*E*)-1h** and **(*Z*)-1h** was observed.

Azetidine compounds are widely found in natural products and biologically active compounds.[18] Then, we expanded our studies to the synthesis of these compounds through intramolecular [2 + 2] cycloaddition with oximes or hydrazones,[18] catalyzed by gold(III)-MOF photosensitizers. Following the modified reaction conditions reported by Schindler and co-workers,[19] **UiO-68[Au1]$_{4.5\%}$** was found to smoothly convert substrates **3a–3f** into azetidine-containing bicyclic products **4a–4f** in a short irradiation time of up to 2 h. The desired azetidines **4a–4f** were formed in high-to-excellent yields (83–98%). Cyclization of oximes **3a–3c** and **3e** yielded azetidine products (**4a–4c** and **4e**) with high diastereoselectivity (>20 : 1 d.r). The structure of one isomer of **4f** was verified by X-ray crystallographic analysis (Table 3). In addition, Stern–Volmer studies were performed on **Au1** by increasing **3d** (as a representative example) concentration, and the large k_q value of 3.0×10^9 dm^3 mol^{-1} s^{-1} confirmed the efficient quenching of the **Au1** excited state by **3d** (Fig. 4a).

Table 3 Light-driven azetidine formation mediated by UiO-68[Au1]$_{4.5\%}$.[a]

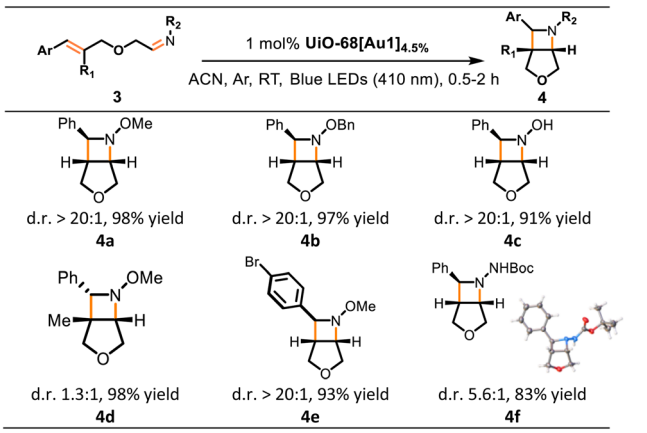

[a] Conditions: reactions were performed with 0.1 mmol of **3a–3f** (used as mixtures of *E*/*Z* oxime or hydrazone isomers) and 5 mg of **UiO-68[Au1]$_{4.5\%}$** in MeCN (2 mL) at room temperature under argon and 410 nm irradiation for 0.5–2 h; product yields and diastereomeric ratios (d.r.) were determined by ^{1}H NMR analysis from the crude reaction mixture using chlorodiphenylmethane as an internal standard. The single-crystal structure of product **4f** is presented.

Table 4 UiO-68[Au1]$_{4.5\%}$-catalyzed homo and cross [2 + 2] dimerization of alkenes[a]

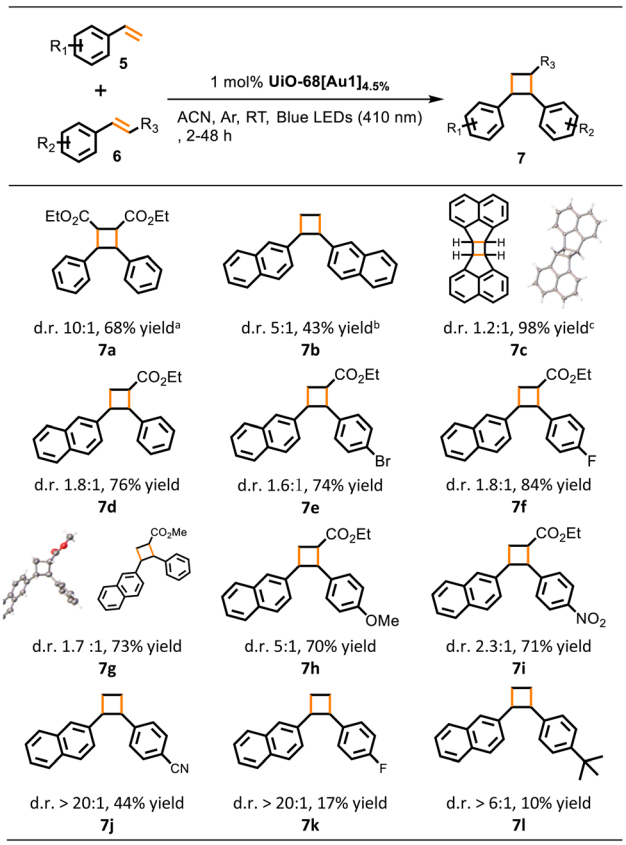

[a] Conditions: reactions (homodimerization for **7a–7c**) were carried out with 0.2 mmol of 2-vinylnaphthalene, **6a** or **6c** and 5 mg of **UiO-68[Au1]$_{4.5\%}$** in MeCN (2 mL) at room temperature under argon and 410 nm irradiation for 30 h[a]/16 h[b]/2 h[c]; reactions (cross dimerization for **7d–7l**) were performed with 0.1 mmol of 2-vinylnaphthalene, 0.3 mmol of aryl terminal alkene or methyl/ethyl cinnamate, and 1 mol% **UiO-68[Au1]$_{4.5\%}$** in MeCN (2 mL) at room temperature under argon and 410 nm irradiation for 3 h; product yields and diastereomeric ratios (d.r.) were determined by ^{1}H NMR analysis from the crude reaction mixture using chlorodiphenylmethane as an internal standard. The crystal structures of anti-**7c**[15e] and **7g** are presented.

The intermolecular [2 + 2] photocycloaddition reaction provides a direct and straightforward method for the synthesis of four-membered cyclic lead compounds using readily available starting materials. However, cycloadditions performed in an intermolecular manner are more challenging than intramolecular reactions. After confirming the applicability of the gold(III)-MOF in the [2 + 2] photocycloaddition of alkenes to synthesize cyclobutane, we studied the homo-coupling [2 + 2] cycloaddition reactions of ethyl cinnamate **6a**, 2-vinylnaphthalene, and cyclic alkene **6c** (Table 4). Significant phosphorescence quenching was observed for **Au1** when substrate **6a** or 2-vinylnaphthalene was added, with a large k_q of (8.7–11) × 10^9 dm^3 mol^{-1} s^{-1} (Fig. 4a). Under optimal reaction conditions, that is, utilizing 1 mol% **UiO-68[Au1]$_{4.5\%}$**, 410 nm irradiation, and MeCN as solvent, homodimerization of **6a** and **6c** led to the formation of cyclobutane in a yield of 68% (**7a**) and as high as 98% (**7c**). However, complete conversion of 2-vinylnaphthalene was observed with an overall product yield of 43% only (**7b**).

Encouraged by the promising results of the homo-coupling cycloaddition, we proceeded to study the cross-coupling [2 + 2] cycloaddition reactions catalyzed by **UiO-68[Au1]$_{4.5\%}$** (Table 4). We selected the heterocycloaddition of 2-vinylnaphthalene with ethyl cinnamate as the benchmark reaction. 2-Vinylnaphthalene was used as a limited substrate, and the ratio of 2-vinylnaphthalene to ethyl cinnamate was optimized to 1 : 3. After 3 h of irradiation under dilute conditions (0.05 mol dm^{-3} of 2-vinylnaphthalene), the yield of product **7d** was 76%. For methyl cinnamate, the yield of product **7g** was 73%, which was comparable to the yield of **7d** (76%) when using ethyl cinnamate. *Para*-functionalized ethyl cinnamate with halogens (bromo and fluoro), electron-donating groups (*i.e.* OMe), or electron-withdrawing groups (*i.e.*, NO_2) is well-tolerated and the corresponding cross-coupled products (**7e**, **7f**, **7h**, and **7i**) were obtained in high yields (71–84%). Compared with previous reports using copper(I)-based MOFs[15c] or iridium(III) photocatalysts,[15d] gold(III)-MOF catalyzed coupling reactions between two different aryl alkenes occurred in significantly shorter irradiation times. In these cross [2 + 2] dimerization reactions of alkenes, small amounts of homo-coupling side products containing ester groups were found in 5–18% yields (see the ESI†), and trace amounts of **7b** were detected. The **UiO-68[Au1]$_{4.5\%}$**-catalyzed homocycloaddition of vinylbenzene did not occur, and only trace amounts of vinylbenzene conversion were observed. This result may be due to the relatively high triplet energy of vinylbenzene. In addition, the cross photo-cycloaddition reaction of 2-vinylnaphthalene with other substituted styrenes was also studied. After irradiation at 410 nm for 3 h, the corresponding cross-cycloaddition products **7j**, **7k**, and **7l** were obtained in yields of 10–44% (Table 4).

Given the ability of these gold(III)-MOFs to generate $^1O_2$ (Fig. 3e), which is known for its utility in oxidation reactions, our focus shifted to exploring the catalytic activity of **UiO-68[Au1]$_{4.5\%}$** in photochemical oxidation reactions under oxygen-saturated conditions. The use of $^1O_2$ has been reported to promote the oxidation of secondary amines to imines and the selective partial oxidation of sulfides to sulfoxides.[1a,b,20] **UiO-68[Au1]$_{4.5\%}$** delivered decent photocatalytic performance for these two oxidation reactions. With 1 mol% **UiO-68[Au1]$_{4.5\%}$**, irradiation of oxygen-saturated solutions containing dibenzylamine or methyl(*p*-tolyl)sulfane can form the desired product in an excellent yield (90–95%; **8a**, **8b**) (Scheme 3).

We further extended the study of gold(III)-MOFs to light-driven aerobic C–H phosphorization of tertiary amines with phosphite esters. For 2-phenyl-1,2,3,4-tetrahydroisoquinoline, its α-C–H bond is oxidized by $^1O_2$ to form iminium ions,[21] which are easily captured by nucleophiles such as dialkyl phosphates. This results in a new bond being installed directly in the α-position of the amine. In this work, 1 mol% **UiO-68[Au1]$_{4.5\%}$** catalyzed the aerobic C–H phosphorization reaction of 2-phenyl-1,2,3,4-tetrahydroisoquinoline in O_2-saturated methanol under light irradiation; phosphonated products containing various dialkyl phosphonates were formed, with a yield of 76–97% (**8c–8h**, Scheme 3). When using air-filled methanol, the product yield of **8c** (93%) was slightly lower than that (97%) achieved under oxygen-saturated conditions (Table S7†). Control experiments confirmed that light, photocatalysts, and oxygen are all necessary for this reaction to proceed. **UiO-68[Au1]$_{4.5\%}$** showed good recyclability and maintained a high conversion of 88% after three consecutive catalytic cycles. The excellent recyclable photocatalytic performance of gold(III)-MOF may be attributed to its robust framework under the photocatalytic reaction conditions, as evidenced by PXRD (Fig. S27†).

To evaluate the potential of gold(III)-MOFs to catalyze photoredox transformations, we selected the reductive cyclization of **9a** as the benchmark reaction. In the presence of **UiO-68[Au1]$_{4.5\%}$** (1 mol%) and stoichiometric diisopropylamine (DIPEA, 2 equiv.), which serves as both a sacrificial electron donor and a hydrogen atom source, the cyclic compound **10a** was obtained in 71% yield in the MeCN/MeOH mixture (1 : 1 v/v) under an argon atmosphere and visible light irradiation. By adding an additional hydrogen donor, 1,4-cyclohexadiene (1,4-CHD, 2 equiv.), the yield of **10a** was increased to 97%. Control experiments showed that when the reaction was carried out without light, DIPEA, or **UiO-68[Au1]$_{4.5\%}$**, no cyclization product **10a** was produced, as shown in Table S8.† Stern–Volmer quenching experiments were performed on **Au1** with increasing concentration of DIPEA or **9a**. Significant emission quenching of **Au1** by DIPEA was observed ($k_q = 7.7 \times 10^9$ dm^3 mol^{-1} s^{-1}, Fig. S28†), whereas no detectable emission quenching of **Au1** was found in the presence of **9a**. Electrochemical studies indicate that the oxidation of DIPEA (E_{pa} = +0.8 V *versus* SCE at 100 mV s^{-1}, Fig. S31†) by the excited state of **Au1** (E(Au*/Au$^-$) = +1.29 V *versus* SCE) is thermodynamically favourable. No oxidation waves for **Au1** were recorded within the potential window of DMF, which makes it difficult to predict the excited state oxidation potential of **Au1** (E(Au$^+$/Au*)). However, the absence of emission quenching of **Au1** by alkyl bromide **9a** excludes the possibility of reduction of 9a by **Au1***.

Combined analysis of emission quenching experiments and electrochemical studies suggests that reductive quenching of **Au1*** by DIPEA initiates the reaction, rather than oxidative quenching of **Au1*** by alkyl bromides, as illustrated in Fig. S29.† Bromoalkanes have reduction potentials of around −1.9 to −2.5 V *versus* SCE.[22] In path A (Fig. S29†), the reduced gold(III) intermediate, [Au^{III}]$^-$, is a strong reducing agent that can promote the reductive cleavage of carbon–bromide bonds to generate carbon-centered radical intermediates. This activation also facilitates the regeneration of the gold(III) photo-catalyst. The resulting alkyl radical then undergoes intramolecular carbon–carbon bond formation reactions.

Alternatively, the α-aminoalkyl radical (intermediate II) derived from DIPEA, generated by reductive quenching of **Au1***, can also serve as a halogen-atom transfer (XAT) reagent.[23] The XAT process between the α-aminoalkyl radical and the alkyl bromide would produce a carbon radical and an iminium salt, as shown in Fig. S30† (path B). The alkyl radical formed by subsequent intramolecular cyclization can be reduced by [Au^{III}]$^-$ to produce a carbanion intermediate, which is then protonated to give the desired cyclic product. To obtain more information on this possibility, we performed cyclic voltammetry experiments on **9a** and DIPEA. At a scan rate of 20–100 mV s^{-1}, DIPEA displays an irreversible oxidation wave located at around 0.73–0.80 V *versus* SCE; this anodic peak current does not increase with the addition of **9a** (approximately 10 equivalents relative to DIPEA; 50 mM of **9a** is the same concentration as the reaction conditions used) (Fig. S31†). If this XAT process occurs, the oxidized DIPEA species will be consumed through the reaction with the substrate **9a**, which will result in an increase in the anodic peak current after the addition of **9a**. Although this alternative pathway is unlikely to be supported based on the current data (Fig. S31†), the reaction between the oxidized DIPEA species and substrate **9a** may be slow compared to the CV scanning times, resulting in no detectable increase in the anodic peak current upon addition of **9a**. From a mechanistic perspective, this alternative reaction pathway (Fig. S30†) cannot be ruled out.

Having established the optimized reaction conditions, we proceeded with the investigation of the substrate scope (Table 5, **9b–9f**). Respective cyclic compounds (**10c–10f**) were obtained in high yields (90–97%) within short irradiation times of up to 2 h.

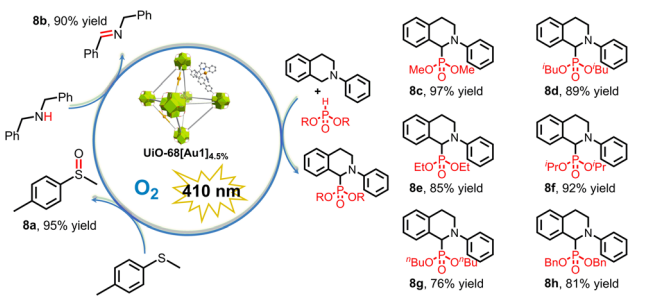

Scheme 3 Visible-light-driven oxidative organic transformations using UiO-68[Au1]$_{4.5\%}$ performed in MeCN.

Table 5 Visible-light-promoted reductive cyclization of alkyl halides facilitated by UiO-68[Au1]$_{4.5\%}$[a]

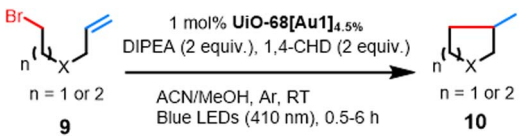

Entry	Substrate		Product		Conversion; yield
1	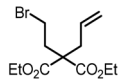	**9a**	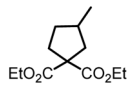	**10a**	99%; 97%
2	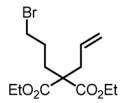	**9b**	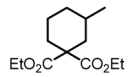	**10b**	95%; 85%
3	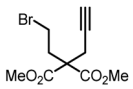	**9c**	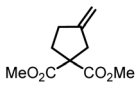	**10c**	99%; 96%
4	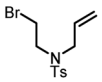	**9d**		**10d**	99%; 97%
5	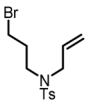	**9e**		**10e**	95%; 90%
6	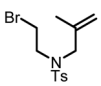	**9f**		**10f**	99%; 95%

[a] Conditions: **9a–9f** (0.1 mmol), diisopropylamine (DIPEA) (0.2 mmol), 1,4-cyclohexadiene (1,4-CHD) (0.2 mmol), and **UiO-68[Au1]$_{4.5\%}$** (5 mg) in a MeCN/MeOH mixture (1 : 1, 1 mL each) at room temperature under argon and 410 nm irradiation for 0.5–6 h; conversions and product yields were determined by ^{1}H NMR analysis from the crude product using chlorodiphenylmethane as an internal standard.

The reaction catalyzed by **UiO-68[Au1]$_{4.5\%}$** exhibits good functional group tolerance, allowing the formation of five-membered and six-membered rings (**10d**, **10e**), radical cyclization of bromoalkynes (*i.e.*, **10c**), and cyclization of sterically demanding bromoalkenes (*i.e.*, **10f**). It is worth noting that the conversion of **9b** into the corresponding cyclic product **10b** required a prolonged irradiation time of 6 h, and the yield was 85%. PXRD analysis confirmed the structural integrity of the MOFs after photolysis under amine-based catalytic conditions (Fig. S32†).

Conclusions

Two novel gold(III)-functionalized MOFs, including **UiO-68[Au1]$_{1.2–4.5\%}$** and **UiO-68[Au2]$_{2.6\%}$**, were developed following a mixed-linker synthetic strategy. The gold(III) emitter **Au1** grafted onto the MOF demonstrates a longer phosphorescence lifetime than its homogeneous counterpart, reaching approximately 110 μs under argon and 12 μs under air at room temperature when suspended in MeCN. The extended lifetime is attributed to the localization of gold(III) complexes within the MOF nanocages, which is supported by gas sorption measurements. The extended emission lifetime provides benefits for light-driven organic transformations that rely on energy transfer or electron transfer mechanisms mediated by photo-excited catalysts. The heterogeneous photocatalyst **UiO-68[Au1]$_{4.5\%}$** shows good performance in intramolecular and intermolecular [2 + 2] cycloaddition reactions, singlet oxygen-sensitized oxidation reactions, and reductive cyclization of alkyl bromides. Furthermore, the gold(III)-MOF catalyst exhibits remarkable recyclability, as it can be easily separated and reused for ten consecutive reaction cycles without significant reduction in catalytic efficiency. The yields of the cyclobutane product remain high, maintaining around 90% after ten cycles of reuse. This excellent recyclability demonstrates the stability and robustness of the gold(III)-MOF photocatalyst reported in this work, which are key features for practical applications requiring long-term operation and reuse of the catalyst. This work highlights the great potential of heterogeneous gold(III)-MOFs as versatile catalytic platforms for photo-redox or energy transfer organic transformations under visible light irradiation, helping to develop milder and more sustainable chemical production.

Data availability

The data that support the findings of this study are available in the ESI† of this article.

Author contributions

C.-M. Che conceived and supervised the project. J.-R. Chen designed and synthesized gold(III)-MOFs, and conducted the characterization and catalytic studies of the developed MOFs. D. Zhou performed the photophysical and mechanistic studies. J.-R. Chen and D. Zhou wrote the original draft of the manuscript. D. Zhou and C.-M. Che revised and refined the final manuscript. J.-R. Chen, D. Zhou, Y. Liu, X.-C. Huang, and C.-M. Che provided lead contributions to data analysis and project discussion. X.-C. Huang, M. Li and Y. Xiao offered suggestions on MOF synthesis and characterization. Y. Xiao provided assistance in solving the X-ray crystal structure of **Me-TPDC-[Au1]**. All authors have read and approved the published version of the manuscript.

Conflicts of interest

There are no conflicts to declare.

Acknowledgements

This work was supported by a research grant from the Innovation and Technology Commission (HKSAR, China) to the State Key Laboratory of Synthetic Chemistry, The University of Hong Kong, Hong Kong Research Grants Council (General Research Fund, HKU 17305521 and 17309823), “Laboratory for Synthetic Chemistry and Chemical Biology” funded by the

Health@InnoHK of Innovation and Technology Commission (HKSAR, China), the Guangdong Major Project of Basic and Applied Basic Research (2019B030302009), the Key (Guangdong-Hong Kong Joint) Laboratory for Preparation and Application of Ordered Structural Materials of Guangdong Province (2023B1212120011), the National Natural Science Foundation of China (22071142), and the Special Fund Project for Science and Technology Innovation Strategy of Guangdong Province (STKJ2023077). The photophysical measurements were conducted in part using the instruments from the Hong Kong Quantum AI Lab Limited funded by the AIR@InnoHK Program of Hong Kong SAR Government. The authors also thank the Southern University of Science and Technology for financial support.

Notes and references

1 (*a*) W.-P. To, G. S.-M. Tong, W. Lu, C. Ma, J. Liu, A. L.-F. Chow and C.-M. Che, *Angew. Chem., Int. Ed.*, 2012, **51**(11), 2654–2657; (*b*) W.-P. To, K. T. Chan, G. S. M. Tong, C. Ma, W.-M. Kwok, X. Guan, K.-H. Low and C.-M. Che, *Angew. Chem., Int. Ed.*, 2013, **52**(26), 6648–6652; (*c*) W.-P. To, G. S. M. Tong, C.-W. Cheung, C. Yang, D. Zhou and C.-M. Che, *Inorg. Chem.*, 2017, **56**(9), 5046–5059.

2 (*a*) M. Idris, S. C. Kapper, A. C. Tadle, T. Batagoda, D. S. M. Ravinson, O. Abimbola, P. I. Djurovich, J. Kim, C. Coburn, S. R. Forrest and M. E. Thompson, *Adv. Opt. Mater.*, 2021, **9**(8), 2001994; (*b*) X. Yang, H. Guo, B. Liu, J. Zhao, G. Zhou, Z. Wu and W.-Y. Wong, *Adv. Sci.*, 2018, **5**(5), 1701067; (*c*) Y. Wu, C. Yang, J. Liu, M. Zhang, W. Liu, W. Li, C. Wu, G. Cheng, Q. Yang, G. Wei and C.-M. Che, *Chem. Sci.*, 2021, **12**(30), 10165–10178.

3 (*a*) É. Whelan, F. W. Steuber, T. Gunnlaugsson and W. Schmitt, *Coord. Chem. Rev.*, 2021, **437**, 213757; (*b*) A. Bavykina, N. Kolobov, I. S. Khan, J. A. Bau, A. Ramirez and J. Gascon, *Chem. Rev.*, 2020, **120**(16), 8468–8535; (*c*) Y.-H. Luo, L.-Z. Dong, J. Liu, S.-L. Li and Y.-Q. Lan, *Coord. Chem. Rev.*, 2019, **390**, 86–126; (*d*) J. Lee, O. K. Farha, J. Roberts, K. A. Scheidt, S. T. Nguyen and J. T. Hupp, *Chem. Soc. Rev.*, 2009, **38**(5), 1450–1459; (*e*) K. Manna, T. Zhang, F. X. Greene and W. Lin, *J. Am. Chem. Soc.*, 2015, **137**(7), 2665–2673.

4 (*a*) H. Furukawa, K. E. Cordova, M. O'Keeffe and O. M. Yaghi, *Science*, 2013, **341**(6149), 1230444; (*b*) H. Deng, S. Grunder, K. E. Cordova, C. Valente, H. Furukawa, M. Hmadeh, F. Gándara, A. C. Whalley, Z. Liu, S. Asahina, H. Kazumori, M. O'Keeffe, O. Terasaki, J. F. Stoddart and O. M. Yaghi, *Science*, 2012, **336**(6084), 1018–1023; (*c*) H. Deng, C. J. Doonan, H. Furukawa, R. B. Ferreira, J. Towne, C. B. Knobler, B. Wang and O. M. Yaghi, *Science*, 2010, **327**(5967), 846–850; (*d*) M. Eddaoudi, J. Kim, N. Rosi, D. Vodak, J. Wachter, M. O'Keeffe and O. M. Yaghi, *Science*, 2002, **295**(5554), 469–472.

5 (*a*) D. Dang, P. Wu, C. He, Z. Xie and C. Duan, *J. Am. Chem. Soc.*, 2010, **132**(41), 14321–14323; (*b*) E. D. Metzger, C. K. Brozek, R. J. Comito and M. Dincă, *ACS Cent. Sci.*, 2016, **2**(3), 148–153; (*c*) C.-D. Wu, A. Hu, L. Zhang and W. Lin, *J. Am. Chem. Soc.*, 2005, **127**(25), 8940–8941.

6 (*a*) J.-D. Xiao, R. Li and H.-L. Jiang, *Small Methods*, 2023, **7**(1), 2201258; (*b*) A. Corma, H. García and F. X. Llabrés i Xamena, *Chem. Rev.*, 2010, **110**(8), 4606–4655.

7 C.-Y. Sun, W.-P. To, X.-L. Wang, K.-T. Chan, Z.-M. Su and C.-M. Che, *Chem. Sci.*, 2015, **6**(12), 7105–7111.

8 J. S. Lee, E. A. Kapustin, X. Pei, S. LIopis, O. M. Yaghi and F. D. Toste, *Chem*, 2020, **6**(1), 142–152.

9 (*a*) B. Ma, Q. Xia, D. Wang, J.-K. Jin, Z. Li, Q.-J. Liang, M.-Y. Sun, D. Liu, L.-J. Liu, H.-X. Shu, J. Yang, D. Li and J. He, *Angew. Chem., Int. Ed.*, 2023, **62**(21), e202300233; (*b*) H. Fei and S. M. Cohen, *J. Am. Chem. Soc.*, 2015, **137**(6), 2191–2194; (*c*) X. Yu and S. M. Cohen, *J. Am. Chem. Soc.*, 2016, **138**(38), 12320–12323.

10 (*a*) X. Ye and D. Liu, *Cryst. Growth Des.*, 2021, **21**(8), 4780–4804; (*b*) J. H. Cavka, S. Jakobsen, U. Olsbye, N. Guillou, C. Lamberti, S. Bordiga and K. P. Lillerud, *J. Am. Chem. Soc.*, 2008, **130**(42), 13850–13851; (*c*) A. Schaate, P. Roy, A. Godt, J. Lippke, F. Waltz, M. Wiebcke and P. Behrens, *Chem.–Eur. J.*, 2011, **17**(24), 6643–6651; (*d*) C. Tan, X. Han, Z. Li, Y. Liu and Y. Cui, *J. Am. Chem. Soc.*, 2018, **140**(47), 16229–16236.

11 M. Nishio, *Phys. Chem. Chem. Phys.*, 2011, **13**(31), 13873–13900.

12 (*a*) M. P. Suh, H. J. Park, T. K. Prasad and D.-W. Lim, *Chem. Rev.*, 2012, **112**(2), 782–835; (*b*) J. L. C. Rowsell, J. Eckert and O. M. Yaghi, *J. Am. Chem. Soc.*, 2005, **127**(42), 14904–14910; (*c*) Y. H. Hu and L. Zhang, *Adv. Mater.*, 2010, **22**(20), E117–E130.

13 (*a*) V. K.-M. Au, K. M.-C. Wong, N. Zhu and V. W.-W. Yam, *J. Am. Chem. Soc.*, 2009, **131**(25), 9076–9085; (*b*) J. J. Yan, A. L.-F. Chow, C.-H. Leung, R. W.-Y. Sun, D.-L. Ma and C.-M. Che, *Chem. Commun.*, 2010, **46**(22), 3893–3895.

14 (*a*) M. R. van der Kolk, M. A. C. H. Janssen, F. P. J. T. Rutjes and D. Blanco-Ania, *ChemMedChem*, 2022, **17**(9), e202200020; (*b*) C. Hui, Y. Liu, M. Jiang and P. Wu, *Trends Chem.*, 2022, **4**(8), 677–681; (*c*) V. M. Dembitsky, *J. Nat. Med.*, 2008, **62**, 1–33.

15 (*a*) Z. Lu and T. P. Yoon, *Angew. Chem., Int. Ed.*, 2012, **51**(41), 10329–10478; (*b*) E. A. Martynova, V. A. Voloshkin, S. G. Guillet, F. Bru, M. Beliš, K. V. Hecke, C. S. J. Cazin and S. P. Nolan, *Chem. Sci.*, 2022, **13**(23), 6852–6857; (*c*) J. Guo, W. Y. Tang, Z. Li, X. Wu, L.-J. Liu, W.-P. To, H.-X. Shu, K.-H. Low, P. C. Y. Chow, T. W. B. Lo and J. He, *Nat. Catal.*, 2024, **7**(3), 307–320; (*d*) Z. Liu, C. Zhou, T. Lei, X.-L. Nan, B. Chen, C.-H. Tung and L.-Z. Wu, *CCS Chem.*, 2019, **2**(1), 582–588; (*e*) J. Guo, Y.-Z. Fan, Y.-L. Lu, S.-P. Zheng and C.-Y. Su, *Angew. Chem., Int. Ed.*, 2020, **59**(22), 8661–8669.

16 (*a*) M. Riener and D. A. Nicewicz, *Chem. Sci.*, 2013, **4**(6), 2625–2629; (*b*) M. A. Ischay, M. S. Ament and T. P. Yoon, *Chem. Sci.*, 2012, **3**(9), 2807–2811.

17 T. Ni, R. A. Caldwell and L. A. Melton, *J. Am. Chem. Soc.*, 1989, **111**(2), 457–464.

18 (*a*) A. Brown, T. B. Brown, A. Calabrese, D. Ellis, N. Puhalo, M. Ralph and L. Watson, *Bioorg. Med. Chem. Lett.*, 2010,

20(2), 516–520; (*b*) D. J. St. Jean Jr and C. Fotsch, *J. Med. Chem.*, 2012, **55**(13), 6002–6020; (*c*) Y.-Z. Zhu, B. M. Johnson and T. J. Yang, *AAPS J.*, 2008, **10**, 178–192.

19 M. R. Becker, A. D. Richardson and C. S. Schindler, *Nat. Commun.*, 2019, **10**(1), 5095.

20 (*a*) T. N. Zehnder, O. Blacque and K. Venkatesan, *Dalton Trans.*, 2014, **43**(31), 11959–11972; (*b*) E. Skolia, P. L. Gkizis and C. G. Kokotos, *Org. Biomol. Chem.*, 2022, **20**(29), 5836–5844.

21 M. Rueping, S. Zhu and R. M. Koenigs, *Chem. Commun.*, 2011, **47**(30), 8679–8681.

22 (*a*) G. Revol, T. McCallum, M. Morin, F. Gagosz and L. Barriault, *Angew. Chem., Int. Ed.*, 2013, **52**(50), 13342–13345; (*b*) M. Zidan, T. McCallum, R. Swann and L. Barriault, *Org. Lett.*, 2020, **22**(21), 8401–8406; (*c*) H. Tran, T. McCallum, M. Morin and L. Barriault, *Org. Lett.*, 2016, **18**(17), 4308–4311.

23 (*a*) L.-Q. Huang, D.-Y. Yang, C.-L. Dong, Y.-H. He and Z. Guan, *Adv. Synth. Catal.*, 2023, **365**(15), 2553–2559; (*b*) Y.-L. Su, L. Tram, D. Wherritt, H. Arman, W. P. Griffith and M. P. Doyle, *ACS Catal.*, 2020, **10**(22), 13682–13687; (*c*) R. K. Neff, Y.-L. Su, S. Liu, M. Rosado, X. Zhang and M. P. Doyle, *J. Am. Chem. Soc.*, 2019, **141**(42), 16643–16650; (*d*) X.-Y. Wang, Y.-Q. He, Y. Zhou, L. Lu, X.-R. Song, Z.-Z. Zhou, W.-F. Tian and Q. Xiao, *Org. Lett.*, 2023, **25**(21), 3847–3852; (*e*) Y. Guo, J. Zhu, Y. Wang, Y. Li, H. Hu, P. Zhang, J. Xu and W. Li, *ACS Catal.*, 2024, **14**(2), 619–627.

